

Dual Dimensions Geometric Representation Learning Based Document Dewarping

Heng Li, Qingcai Chen, *Member, IEEE*, Xiangping Wu

Abstract—Document image dewarping remains a challenging task in the deep learning era. While existing methods have improved by leveraging text line awareness, they typically focus only on a single horizontal dimension. In this paper, we propose a fine-grained deformation perception model that focuses on Dual Dimensions of document horizontal-vertical-lines to improve document Dewarping called *D2Dewarp*. It can perceive distortion trends in different directions across document details. To combine the horizontal and vertical granularity features, an effective fusion module based on X and Y coordinate is designed to facilitate interaction and constraint between the two dimensions for feature complementarity. Due to the lack of annotated line features in current public dewarping datasets, we also propose an automatic fine-grained annotation method using public document texture images and an automatic rendering engine to build a new large-scale distortion training dataset. The code and dataset will be publicly released. On public Chinese and English benchmarks, both quantitative and qualitative results show that our method achieves better rectification results compared with the state-of-the-art methods. The dataset will be publicly available at <https://github.com/xiaomore/DocDewarpHV>

Index Terms—Computer vision, Deep learning, Geometric representation learning, Document image rectification.

I. INTRODUCTION

In recent years, the widespread usage of mobile electronic devices, such as smartphones and cameras, has led people to rely increasingly on capturing electronic documents through photography. However, issues such as device placement, lighting conditions, and paper deformation often result in varying degrees of distortion in the captured document images. As a result, extracting useful information from these images becomes challenging, posing difficulties for tasks such as text content recognition [1]–[10], document understanding [11]–[16]. Consequently, the rectification of distorted document images has garnered increasing attention from researchers. In this work, we focus on dewarping arbitrarily deformed document images captured in real-world scenarios.

Recently, representation learning-based rectification techniques have significantly enhanced the visualization and readability of distorted document images. These methods employed convolutional neural networks (CNNs) and transformers to learn 2D deformation field (backward map) that maps the warped image to the scanned image, thereby optimizing the geometric dewarping task [17]–[32]. For example, DocUNet

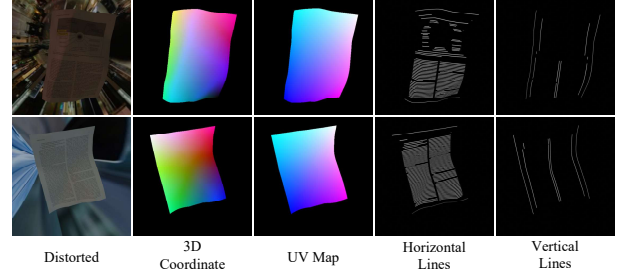


Fig. 1. Visualization of the synthetic warped dataset. The first column is the distorted document image with complex background. *3D Coordinate*: the position of each pixel of the distorted image in three-dimensional space. *UV map*: maps the 3D surface to the location of the 2D coordinate system texture map. *Horizontal Lines*: in addition to text lines, its also include the top and bottom boundaries of documents, tables, figures, and paragraphs. *Vertical Lines*: the left and right boundaries of the deformed document area, tables, figures, and paragraphs.

[17] utilized UNet networks to regress the 2D backward map. DocTr [21] introduced a transformer-based approach to analyze the dependencies among features extracted from warped images. DocReal [28] combined channel and spatial attention to enhance control point prediction to better capture local deformations. These methods utilized CNNs or attention mechanism to directly regress 2D deformation fields.

To enhance correction accuracy, some methods incorporated additional information to assist in dewarping. For instance, DewarpNet [18] utilized a two-stage process involving shape and texture networks to predict 3D coordinates and 2D deformation fields. Similarly, FCN-based [20] adopted fully convolutional networks (FCNs) to estimate pixel displacements, thereby rectified distorted document images and delicately removing backgrounds. DocGeoNet [24] predicted the foreground of distorted images to minimize background interference and uses a multi-layer transformer to capture 3D coordinate features. In terms of local rectification, recent approaches enhanced document readability by focusing on text line regions [23], [24], [27]. Besides, LA-DocFlatten [26] utilized layout information to further refine local rectification in distorted images.

Although these recent advances have proven that text lines [23], [24], [27], layout information [26], and obtaining vertical information from text lines in a rule-based manner [23], can effectively improve image rectification performance, the granularity of these methods is not sufficiently constrained and complementary. The methods that introduce text line information ignore the consideration of tables or figures in the document. The methods guided by layout information treated

Heng Li, Qingcai Chen and Xiangping Wu are with the School of Computer Science and Technology, Harbin Institute of Technology (Shenzhen), Shenzhen University Town, Xili, Shenzhen 518055, China. And Qingcai Chen is also with the PengCheng Laboratory, Shenzhen, China. (e-mail: hengli.lh@outlook.com; qingcai.chen@hit.edu.cn; wxpleduole@gmail.com)

figures, tables or paragraphs as separate categories, lack the mining of finer-grained factors within the category, that is the interaction between text lines within a paragraph.

To alleviate the above issues, we define the deformation representation of the image from two dimensions, horizontal and vertical. For a distorted document image with layout categories, as shown in the Figure 1, we regard the top and bottom boundaries of entire distorted document foreground, tables, figures, paragraphs, and the text lines within the paragraph as lines of horizontal dimension. Similarly, the left and right boundaries of these categories are classified as lines of vertical dimension. Considering the deformation characteristics of lines in both the horizontal and vertical directions of distorted document images, we designed and implemented a fusion module to more effectively learn the mutual constraints and feature complementarity between these two dimension features.

The main contributions of our work are summarized as follows:

- We present a novel end-to-end architecture for dual-dimension geometric representation learning of warped document images, capturing fine-grained deformation trends in both horizontal and vertical directions.
- We design an effective fusion module to integrate distortion features from both dimensions, enhancing their interaction and constraints for optimal feature complementarity.
- We release a new training dataset of distorted document images with more refined annotations in dual dimensions. Experimental results confirm that our method attains state-of-the-art performance. we will publicly release our model and source code to facilitate further research and development.

II. RELATED WORK

The goal of unwarping distorted images extends beyond visual enhancement, encompassing facilitation of downstream tasks like document understanding and text content extraction. Traditional methods for document image rectification typically employ parametric regression, relying on superficial image features such as textlines [33], cylindrical surfaces [34]–[37], and document boundaries [38], [39].

In recent years, various approaches have been proposed for rectifying distorted document images, leveraging deep representation learning and innovative network architectures. Ma *et al.* [17] introduced DocUNet, utilizing synthetic datasets for training, which employed a stacked UNet structure to regress the 2D deformation field. Xie *et al.* [20] proposed a method that predicts pixel displacement with local smoothing constraints and utilized an interpolation technique for sparse mapping conversion. Feng *et al.* [21] pioneered the use of transformer for document dewarping, proposing a rectification model based on foreground extraction. DocScanner [40] employed a recurrent architecture for step-by-step unwarping, maintaining a single estimate of the rectified image. DocTr-plus [41] enhanced DocTr [21] with a hierarchical encoder-decoder structure for multi-scale representation extraction and

parsing. Liu *et al.* [29] proposed DRNet, a coarse-to-fine network and a consistency loss to facilitate document image rectification.

To better focus on either global or local information in the distorted image. Das *et al.* [18] employ UNet to simultaneously model the 3D global coordinates and texture network for warped images using the released Doc3D training data. Li *et al.* [42] proposed a method to stitch patch results into the rectified document by processing in the gradient domain. Similarly, Piece-wise [43] fused local deformation fields with global information by predicting 3D coordinates to enhance dewarped images. Conversely, methods such as DocGeoNet [24] and RDGR [23] integrated text line information with local attributes. FTDR [27] extends these methods by leveraging cross-attention mechanisms focused on the foreground and textline regions. In contrast, LA-DocFlatten [26] incorporates a hybrid segmentation network, utilizing both convolutional neural networks and transformers to extract layout information from documents. This is followed by a regression module designed to predict both global and local UV maps. While our proposed model emphasizes the simultaneous interaction of horizontal and vertical features, not only considering fine-grained local information, but also focusing on the effective fusion and mutual influence between them.

III. PROPOSED METHOD

In this section, we introduce the overall structure of our proposed method for distorted document image dewarping. The architecture of the model is shown in Figure 2. Our network mainly consists of two parts: the horizontal and vertical line segmentation model of the UNet structure with dual decoders, and a lightweight module (HV Fusion Module) that fuses these two line features.

Segment Dual Lines. Drawing on the excellent effect of UNet [44] in the field of image segmentation, we use a similar encoder structure in this part. For an input distorted document image $I \in \mathbb{R}^{H \times W \times C}$, $H=W=448$ is the height and width of the image, and $C=3$ denotes the RGB channels of the source distorted image. It is input into the segmentation model to predict horizontal and vertical lines. The encoder contains five layers. The input image undergoes two 3×3 convolutions, batch normalization (BN) [45], and Rectified Linear Unit (ReLU) activation [46] (ConvBNReLU) in the first layer to extract general feature representations. The remaining four layers are downsampling modules, which consist of maximum pooling and two ConvBNReLU. The feature map output size of the last layer of the encoder is $1/16$ of the input image I . The feature map output by the encoder are recorded as $\{E_1, E_2, E_3, E_4, E_5\}$ with the output size $\{448 \times 448, 224 \times 224, 112 \times 112, 56 \times 56, 28 \times 28\}$ and the channels $\{32, 64, 128, 196, 448\}$. In order to capture the long-distance dependency between feature map elements, we use l layers of self-attention after the encoder, where $l = 4$.

Dual Decoders. Each decoder has four layers with exactly the same structure, upsampling and line prediction modules. Among them, the upsampling module consists of bilinear interpolation and two ConvBNReLU. Line prediction is implemented by a layer of 1×1 convolution and then directly

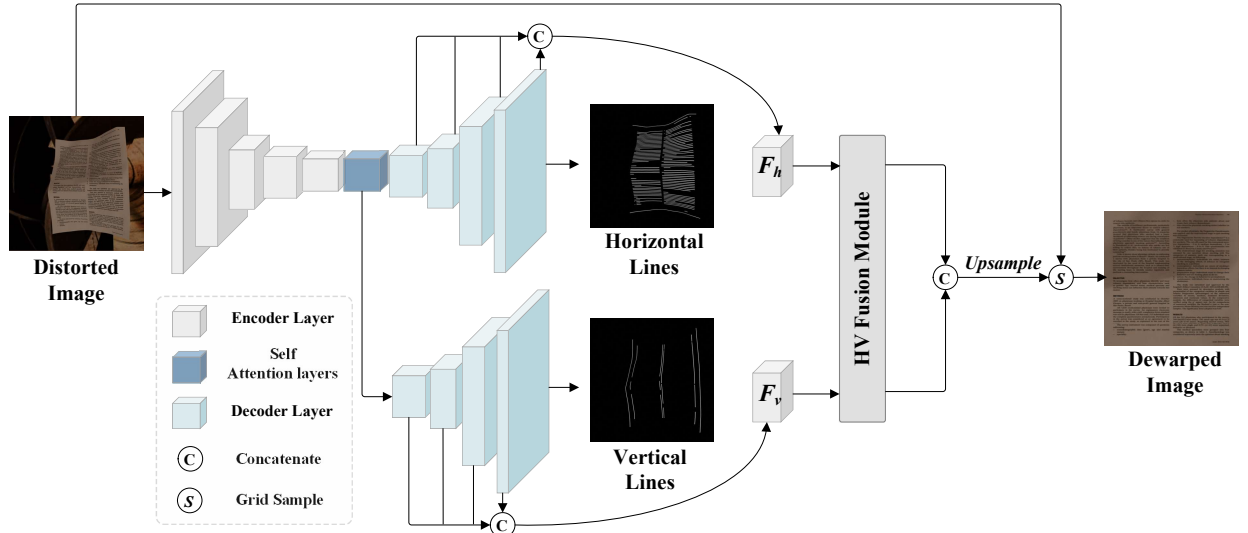


Fig. 2. The architecture of our proposed method *D2Dewarp*. The segmentation model of the UNet structure predicts the two dimensions of lines. The dual decoders share the same encoder. Each layer in the decoder outputs the prediction result of the line, and then the feature map of each layer is resized to one-eighth of the input image and concatenated to obtain F_h and F_v respectively. The HV Fusion Module is used to fuse the feature maps of horizontal and vertical lines. For better visualization, we omit the skip connection line of UNet in this figure.

upsample to the input image size using bilinear interpolation. The output feature map of the decoder layer are recorded as $\{D_1, D_2, D_3, D_4\}$ with the output size $\{56 \times 56, 112 \times 112, 224 \times 224, 448 \times 448\}$ and the channels $\{196, 128, 64, 48\}$. These four feature maps are resized to one eighth of the input image, then concatenated in the channel dimension and input into ConvBNReLU to obtain horizontal and vertical geometric features $F_h \in \mathbb{R}^{56 \times 56 \times 448}$ and $F_v \in \mathbb{R}^{56 \times 56 \times 448}$ respectively.

HV Fusion Module. This module aims to fuse the two geometric features obtained by the segmentation model. Leveraging the pooling operation's ability to aggregate local information on the feature map and inspired by the superiority of coordinate attention in image classification [47], we propose using 2D average pooling to capture local information along the X and Y spatial directions. For feature maps, the so-called X and Y also refer to the two dimensions of width and height. The horizontal F_h and vertical features F_v of the distorted image obtained by the segmentation model correspond to the pooling in the X and Y directions. The module is shown in Figure 3. For F_h and F_v , X and Y two-dimensional average pooling is used to obtain the mixed pooling features:

$$\begin{aligned} F_{h_X}, F_{h_Y} &= AvgPool_X(F_h), AvgPool_Y(F_h) \\ F_{v_Y}, F_{v_X} &= AvgPool_Y(F_v), AvgPool_X(F_v) \\ F_{mix1} &= CAT(F_{h_X}, Trans(F_{v_Y}))_{dim=2} \\ F_{mix2} &= CAT(Trans(F_{h_Y}), F_{v_X})_{dim=2} \end{aligned} \quad (1)$$

where $CAT(\cdot)$ represents feature map concatenation. $Trans(\cdot)$ is dimension transposition.

The mixed attention mechanism is used to capture the long-distance dependencies in the X or Y direction from F_h or F_v respectively. Interacting features from different sources in different directions can achieve the purpose of constraining horizontal and vertical features to each other, thereby making up for their respective shortcomings. The mixed attention here

refers to the attention relationship between features in different directions (X and Y) of the two feature maps. The calculation formulas are as follows:

$$\begin{aligned} F'_{mix1} &= MixedAttention(F_{mix1}) \\ F'_{mix2} &= MixedAttention(F_{mix2}) \\ F'_{h_X}, F'_{v_Y} &= Split(F'_{mix1}) \\ F'_{v_X}, F'_{h_Y} &= Split(F'_{mix2}) \\ F_{cat_X} &= CAT(Conv2d(F'_{h_X}), Conv2d(F'_{v_X})) \\ F_{cat_Y} &= CAT(Conv2d(F'_{h_Y}), Conv2d(F'_{v_Y})) \end{aligned} \quad (2)$$

where $Split(\cdot)$ represents channel separation.

After obtaining the mixed attention features F'_{mix1} and F'_{mix2} , let the features return to different directions of independent line features. In this step, we separate them in the channel dimension. X/Y self attention is used to capture the long-distance dependencies in the X and Y directions from F_h . The same applies to F_v . X/Y self attention here refers to the attention relationship between the features of two line feature maps in the same direction (X or Y). Formulas are as follows, where $Sig(\cdot)$ represents the *Sigmoid* activation function, which normalizes feature values to $[0, 1]$. Concatenate F'_{h_X} and F'_{v_Y} in the channel dimension, and then predict the 2D deformation field \hat{G} through the upsampling module. Here we use the upsampling module of DocTr [21], DocGeoNet [24] and FTDR [27]. The 2D deformation field has two channels, mapping the vertical and horizontal position coordinates between the distorted image pixels and the flat

image.

$$\begin{aligned}
F''_{h-X}, F''_{v-X} &= \text{Split}(\text{X Self Attention}(F_{cat-X})) \\
F''_{h-Y}, F''_{v-Y} &= \text{Split}(\text{Y Self Attention}(F_{cat-Y})) \\
F''_{h-X}, F''_{v-X} &= \text{Sig}(\text{Conv2d}(F''_{h-X})), \text{Sig}(\text{Conv2d}(F''_{v-X})) \\
F''_{h-Y}, F''_{v-Y} &= \text{Sig}(\text{Conv2d}(F''_{h-Y})), \text{Sig}(\text{Conv2d}(F''_{v-Y})) \\
F'_h &= F_h \times F''_{h-X} \times F''_{h-Y} \\
F'_v &= F_v \times F''_{v-X} \times F''_{v-Y}
\end{aligned} \tag{3}$$

In general, the average pooling operation can extract more robust feature representations. The horizontal and vertical characteristics of the lines in the distorted document combined with the coordinate information in the X and Y directions in the feature map help to strengthen the geometric representation of the deformed features. Our experimental results (Table V and Table VI) prove the effectiveness of this fusion module.

Loss function. During the model training process, we predict horizontal and vertical lines with Binary Cross-Entropy (BCE) loss [48]. To optimize the imbalance between the pixel ratio of the line mask and other areas, we use the line loss \mathcal{L}_{line} proposed in RDGR [23] as the loss for predicting horizontal and vertical lines ($\mathcal{L}_{line}^h, \mathcal{L}_{line}^v$). This loss uses the L_2 loss weighted pixel proportions. In order to weight the output of different layers of the UNet decoder, we use different loss weights for each decoder layer. The losses are calculated as follows:

$$\begin{aligned}
\mathcal{L}_{bce}^h &= -\frac{1}{K} \sum_{k=1}^K [y_k^h \log(\hat{y}_k^h) + (1 - y_k^h) \log(1 - \hat{y}_k^h)] \\
\mathcal{L}_{bce}^v &= -\frac{1}{K} \sum_{k=1}^K [y_k^v \log(\hat{y}_k^v) + (1 - y_k^v) \log(1 - \hat{y}_k^v)] \\
\mathcal{L}_{line} &= \sum_{i=1}^L [\mathcal{L}_{line}^h + \mathcal{L}_{line}^v + \frac{1}{2L-i} (\mathcal{L}_{bce}^h + \mathcal{L}_{bce}^v)]
\end{aligned} \tag{4}$$

where K represents the pixel count of the input image, y and \hat{y} respectively are the ground truth and predicted results. L is the number of layers of the decoder. i is the i -th layer of the decoder.

To quantify the image rectification loss of our model during training, we compute the L_1 distance between the predicted deformation field \hat{G} of the warped image and its ground truth G . The calculation is as follows:

$$\mathcal{L}_{rec} = \|G - \hat{G}\|_1 \tag{5}$$

Our model concurrently optimizes lines mask along with 2-dimensional deformation fields in an end-to-end manner. The formula for the overall training loss is presented below:

$$\mathcal{L} = \alpha \mathcal{L}_{rec} + \mathcal{L}_{line} \tag{6}$$

where α represents a hyper-parameter weight, which is assigned a value of 5 to ensure an balance among various loss functions.

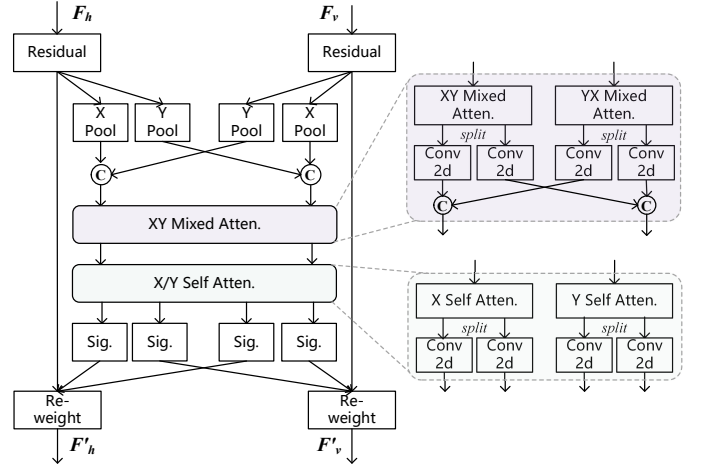


Fig. 3. The HV Fusion Module. F_h and F_v represent the horizontal and vertical feature maps obtained by the segmentation model as the input of this module, respectively. X or Y Pool uses AdaptiveAvgPool2d. Sig. refers to Sigmoid activation function. C denotes concatenation.

IV. EXPERIMENTS

A. Datasets

Since the existing public training dataset Doc3D [18] lacks annotations for horizontal and vertical lines, and obtaining these two lines through visual image processing method will result in several errors. Therefore, we refer to the data synthesis methods of DewarpNet [18], DocMAE [49], and LA-DocFlatten [26]. To synthesize distorted images containing Chinese and English documents as training sets using the public rendering tool blender¹. English documents come from the development set of PubLayNet [50]. Chinese documents are obtained from the CDLA [51], CDDOD [52], and test sets of M6Doc [53]. These document datasets all have layout annotation information. We use the public OCR engine PaddleOCR² to detect the coordinate of text. By merging the boundaries of document page and layout, and information of text lines, the masks with horizontal and vertical lines can be obtained separately. Using the same rendering method to generate distorted results for these two masks and the scanned image.

About 110K warped images are synthesized, named *DocDewarpHV*. Some samples are shown in Figure 1. Table I shows the statistics of our proposed warped training dataset and the comparison with Doc3D [18]. During the synthesis process, we randomly add background as interference. In addition to distorted images, it also contains 3D coordinates, UV map, horizontal and vertical line masks. In order to promote further exploration of document rectification task in the research community, we will open source this training dataset³.

DocUNet Benchmark. The benchmark introduced by Ma *et al.* [17], which is the first application of deep learning in this task. This benchmark has been widely used in recent research, featuring 130 distorted images of documents in

¹<https://pypi.org/project/bpy/>

²<https://github.com/PaddlePaddle/PaddleOCR>

³<https://github.com/xiaomore/DocDewarpHV>

TABLE I

COMPARE DOC3D [18] AND OUR PROPOSED DOCDEWARPHV DATASETS OF DISTORTED DOCUMENT IMAGES. WHERE H-LINE AND V-LINE REPRESENT HORIZONTAL AND VERTICAL LINE ANNOTATIONS, RESPECTIVELY.

Dataset	Image	Resolution	Global Info.		Local Info.		Language	
			3D Coord.	UV Map	H-Line	V-Line	English	Chinese
Doc3D [18]	102,027	448 × 448	✓	✓	✗	✗	✓	✗
DocDewarpHV	114,385	512 × 512	✓	✓	✓	✓	✓	✓

TABLE II

COMPARISONS ON DOCUNET BENCHMARK [17]. “↑” INDICATES THE HIGHER THE BETTER AND “↓” DENOTES THE OPPOSITE. THE BEST PERFORMING RESULT IS SHOWN IN **BOLD** FONT, AND THE SECOND BEST RESULT IS SHOWN WITH AN UNDERLINE.

Method	Venue	MS-SSIM ↑	LD ↓	AD ↓	ED ↓	CER ↓
Distorted	-	0.25	20.51	1.012	2111.56/1552.22	0.5352/0.5089
DocUNet [17]	CVPR’18	0.41	14.19	-	1933.66/1259.83	0.4632/0.3966
DewarpNet [18]	ICCV’19	0.47	8.39	0.426	885.90/525.45	0.2373/0.2102
FCN-based [20]	DAS’20	0.45	7.84	0.434	1792.60/1031.40	0.4213/0.3156
Piece-Wise [43]	ICCV’21	0.49	8.64	0.468	1069.28/743.32	0.2677/0.2623
DocTr [21]	MM’21	0.51	7.76	0.396	724.84/464.83	0.1832/0.1746
DDCP [22]	ICDAR’21	0.47	8.99	0.453	1442.84/745.35	0.3633/0.2626
FDRNet [54]	CVPR’22	<u>0.54</u>	8.21	-	829.78/514.90	0.2068/0.1846
RDGR [23]	CVPR’22	0.50	8.51	0.461	729.52/420.25	0.1717/0.1559
DocGeoNet [24]	ECCV’22	0.50	7.71	0.380	713.94/379.00	0.1821/0.1509
PaperEdge [55]	SIGGRAPH’22	0.47	7.99	0.392	777.76/375.60	0.2014/0.1541
FTDR [27]	ICCV’23	0.50	8.43	0.376	697.52/450.92	0.1705/0.1679
LA-DocFlatten [26]	TOG’23	0.53	<u>6.72</u>	<u>0.300</u>	695.00/391.90	0.1750/0.1530
UVDoc [56]	SIGGRAPH’23	0.55	6.79	0.310	797.92/493.13	0.1975/0.1611
DocTr-Plus [41]	TMM’23	0.51	7.52	-	-/447.47	-/0.1695
DocRes [57]	CVPR’24	0.47	9.37	0.471	912.50/500.27	0.2406/0.1751
DocTLNet [58]	IJDAR’24	0.51	6.70	-	-/377.12	-/0.1504
DocReal [28]	WACV’24	0.50	7.03	0.286	<u>730.96/360.32</u>	<u>0.1909/0.1443</u>
DocScanner [40]	IJCV’25	0.52	7.45	0.334	632.30/390.40	<u>0.1650/0.1490</u>
Ours	-	0.50	7.71	0.349	<u>656.30/351.08</u>	0.1543/0.1338

natural settings, captured using mobile devices. The dataset encompasses a diverse array of document types, including bills, papers, and posters.

DIR300 Benchmark. The dataset assembled and released by Feng *et al.* [24], consists of 300 authentic English document samples, creating a more extensive test set compared to the DocUNet Benchmark dataset [17]. Beyond merely amplifying the degree of document distortion, the dataset encompasses more complex backgrounds and a range of lighting conditions.

DocReal Benchmark. This benchmark [28] contains a total of 200 distorted document images. Compared with DocUNet [17] and DIR300 [24] benchmarks, it is currently the largest number of distorted Chinese documents. Image types cover contracts, bills, and books. These images have complex real backgrounds and various deformations, and have the characteristics of more scenes, greater reality, and larger deformation range.

B. Evaluation metrics

MS-SSIM, LD and AD. Our evaluation employs metrics widely used in prior research [17], [21], [23], [24], [26], [27], [40], [41], [55], [59]. Structural Similarity (SSIM) assesses the similarity between two images based on their luminance, contrast, and structural attributes. Multi-Scale Structural Similarity (MS-SSIM) [60] enhances SSIM by evaluating contrast and structure across multiple scales and measuring luminance only at the final scale. Local Distortion (LD) [61] quantifies

the average local deformation per pixel between the corrected image and an authentic scanned counterpart, utilizing SIFT flow [62] for analysis. Aligned Distortion (AD) [55], building on MS-SSIM and LD, addresses their limitations: MS-SSIM’s sensitivity to minor global changes and LD’s tendency to inaccurately flag errors in texture-lacking regions.

ED and CER. Our method’s dewarping quality on distorted images is assessed using OCR recognition performance. Edit Distance (ED) is defined as the minimum number of operations needed to transform one string into another, including insertions (*i*), deletions (*d*), and substitutions (*s*). Consequently, the Character Error Rate (CER) is calculated using the formula: $(i + d + s)/M$, where *M* represents the total number of characters in the reference string. In alignment with previous methodologies [21], [24], [26], [27], our evaluation on the DocUNet Benchmark involves 50 and 60 images, respectively. Furthermore, the DIR300 dataset’s OCR performance is analyzed using 90 text-rich images, maintaining consistency with these established methods. The CER and ED performance of all 200 images are displayed on the DocReal benchmark.

C. Implementation details

During training, input images are cropped and then resized to 448×448 . Optimization is performed using the AdamW optimizer [63], with a batch size set to 28. The learning rate begins at a maximum of 1×10^{-4} and decreases to a minimum of 1×10^{-7} , employing a cosine learning rate decay strategy.



Fig. 4. The qualitative visualization results of our method and previous methods are compared on the DocUNet benchmark [17]. The first column is the input distorted document image, and the last column is the dewarping result of our method. The middle columns are the effects of other previous methods.

TABLE III
COMPARISONS RECTIFICATION PERFORMANCE ON DIR300 BENCHMARK [24].

Method	MS-SSIM \uparrow	LD \downarrow /AD \downarrow	ED \downarrow /CER \downarrow
Distorted	0.32	39.58/0.771	1500.56/0.5234
DocProj [42]	0.32	30.63/-	958.89/0.3540
DewarpNet [18]	0.49	13.94/0.331	1059.57/0.3557
DocTr [21]	0.62	7.21/0.254	699.63/0.2237
DDCP [22]	0.55	10.95/0.357	2084.97/0.5410
DocGeoNet [24]	0.64	6.40/0.242	664.96/0.2189
PaperEdge [55]	0.58	8.00/0.255	508.73/0.2069
FTDR [27]	0.61	7.68/0.244	652.80/0.2115
DocScanner [40]	0.62	7.06/0.225	562.72/0.1943
LA-DocFlatten [26]	0.65	5.70/0.195	511.13/0.1891
UVDoc [56]	0.62	7.71/0.218	605.24/0.2601
DocRes [57]	0.63	6.81/0.243	764.20/0.2403
DocTLNet [58]	0.66	5.75/-	<u>482.57/0.1767</u>
Ours	<u>0.65</u>	<u>5.73/0.186</u>	466.94/0.1676

TABLE IV
COMPARISONS RECTIFICATION PERFORMANCE ON DocREAL BENCHMARK [28]. THE DATA IN THIS TABLE EVALUATED BY OURSELF FROM THE PUBLIC CODE OR RECTIFIED RESULTS OF PREVIOUS METHODS.

Method	MS-SSIM \uparrow	LD \downarrow /AD \downarrow	ED \downarrow /CER \downarrow
Distorted	0.32	35.79/0.771	1500.56/0.5234
DocTr	0.55	12.68/0.322	208.51/0.2943
DDCP	0.47	16.36/0.449	264.71/0.3300
DocGeoNet	0.55	12.24/0.314	216.68/0.2974
PaperEdge	0.52	11.47/0.303	186.86/0.2451
RDGR	0.54	11.47/0.333	188.00/0.2768
FTDR	0.51	13.25/0.350	217.68/0.2890
DocScanner	0.54	12.36/0.308	196.14/0.2709
UVDoc	0.55	11.40/0.274	203.12/0.2688
DocRes	0.55	11.71/0.330	224.44/0.3087
DocReal	0.56	9.83/0.238	184.54/0.2485
Ours	0.58	8.69/0.227	191.25/0.2588

The model undergoes training for 80 epochs with a warm-up phase of 10,000 steps. Following [21], [24], [26], [40], [59], evaluation metrics MS-SSIM, LD, and AD are computed using Matlab R2019a. OCR performance assessment on the two English benchmarks DocUNet and DIR300 are conducted using Tesseract v5.0.1.2022011 [64] with pytesseract v0.3.8⁴. Since PaddleOCR is open source and available, and has shown excellent performance in Chinese text recognition, we use it for evaluation on the Chinese benchmark DocReal [28].

D. Experimental results

Result on DocUNet Benchmark. We show the comparison between our model and previous rectification methods, as shown in Table II. It can be seen that our network almost

completely surpasses previous methods in terms of CER and ED. Compared with the textline-introducing methods [23], [24], and [27], our method improves the CER by at least 9.5% and 11.3% on 50 and 60 images respectively. Compared with the layout-focused method [26], we outperform by 10.4% on ED and 12.5% on CER for the 60-image test setting. However, our method does not have much advantage in terms of MS-SSIM, LD and ED. According to our observation, the images in this benchmark contain more figures than the other two benchmarks. In fact, it is more difficult to predict the boundary lines of document foreground, figures and tables than text lines. In other words, the features of text lines are more obvious. The boundaries of the document foreground are easily disturbed by the background. The model is not sensitive enough to the boundary perception of figures and tables compared to text lines. Increasing the number of training sets (the 300K training set of the method [28]) or appropriately

⁴<https://pypi.org/project/pytesseract/>

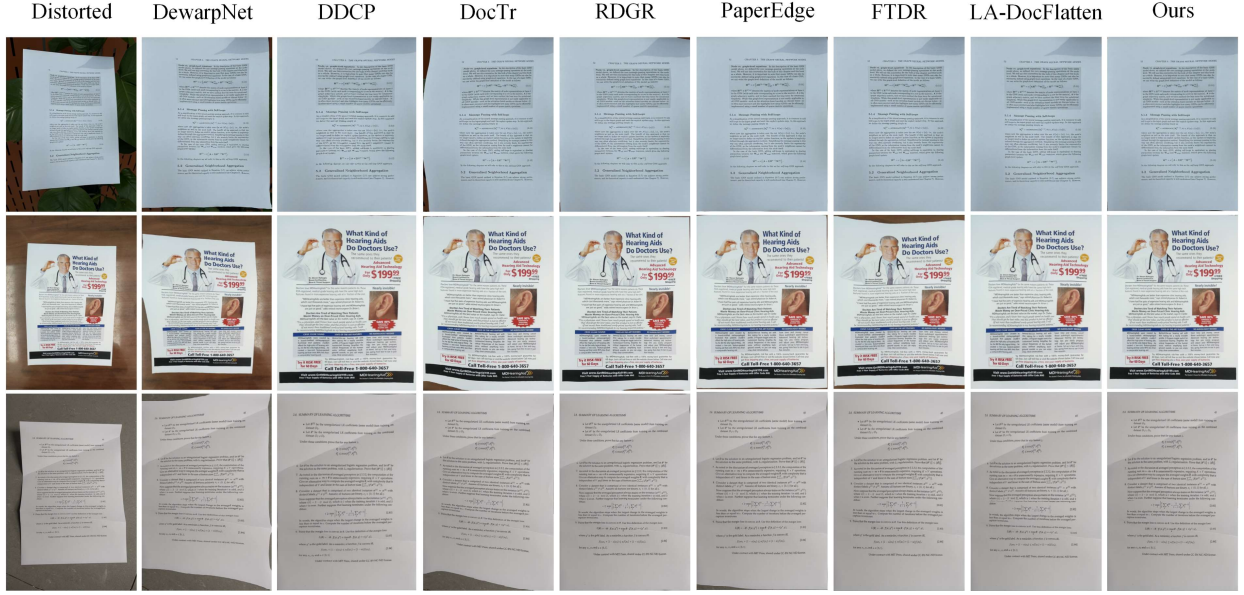


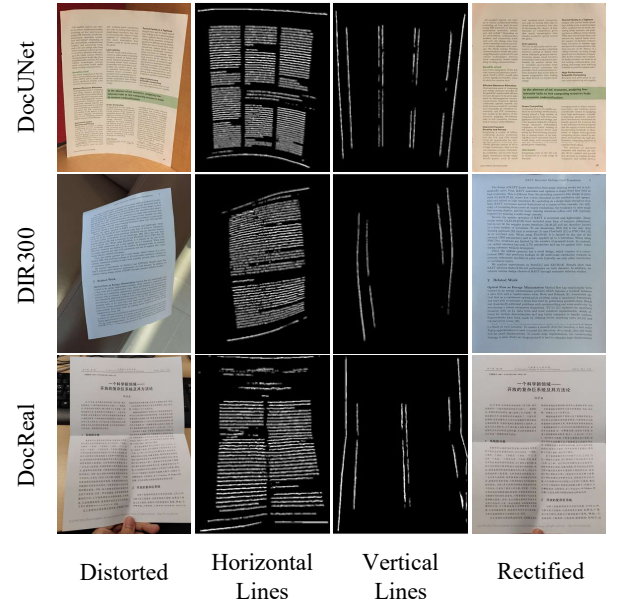
Fig. 5. Qualitative visualization comparison on DIR300 benchmark [24].

increasing the input image resolution may optimize this problem. The qualitative visualization results are shown in Figure 4.

Result on DIR300 Benchmark. As shown in Table III, the best results are achieved for most indicators on DIR300. Compared with the current best method [26], we enhance AD by 4.6%. and on OCR evaluation metrics, our method outperforms the current state-of-the-art method DocTLNet [58] by 3.2% on CER and 5.1% on ED. The warped images in this dataset contain more text content. For rich text distorted images, the denser the text lines, the better the rectification performance of our method. The visualization results of the rectification are shown in Figure 5.

Result on DocReal Benchmark. Table IV shows the quantitative evaluation results of distorted image correction on the DocReal benchmark [28]. Our method brings significant improvements in the three metrics of MS-SSIM (3.6%), LD (11.6%) and AD (4.6%). However, our method still needs to be further improved in ED and CER. In the light of our analysis, there are always differences in line heights between English and Chinese documents, especially text lines. This is a limitation of our method. Perhaps adaptive learnable pooling to accommodate line heights is desirable. In order to intuitively observe the output results of the model for distorted document correction, we show qualitative visualization effects in Figure 9. To more precisely examine the line results predicted and the rectified output by our model, we visualize these two lines as depicted in Figure 6 on three benchmarks. For text-sparse distorted documents, our method effectively distinguishes document foreground from background using detected document boundaries (Figure 7).

Bad Case Analysis. Our proposed approach achieves significant improvements, but there are still some limitations. As shown in Figure 8, the top row is the pictures of camera in the document and the bottom right position has no clear

Fig. 6. **Text-Heavy** Dewarped Results Visualization. The input distorted image (first column), horizontal and vertical line prediction (middle two columns) and rectification results (last column) on DocUNet [17], DIR300 [24] and DocReal [28] benchmarks.

boundary (yellow arrow), which will lead to undetected lines or false detection. The bottom row shows that text lines in the background (red dotted ellipse) and cause the model to misjudge. As a result, the rectified image contains background.

Inference Speed. On the DocUNet benchmark (130 images), our evaluation was conducted on an NVIDIA V100 GPU (32GB) with batch size 16 (24GB memory utilization), completing in 50.13 seconds at an average of 0.39 seconds per image.

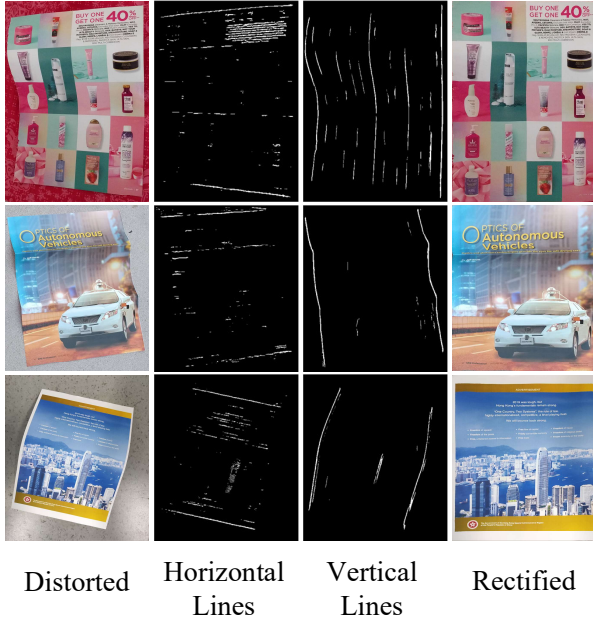
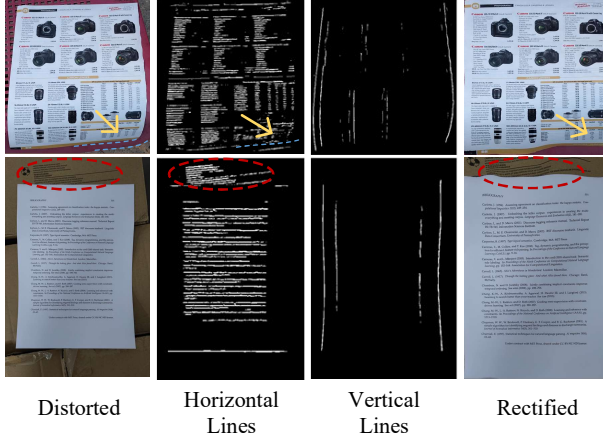
Fig. 7. **Figure-Heavy** (text-sparse) Dewarped Results Visualization.

Fig. 8. Visualization of the bad cases. In the first row, the foreground and background cannot be completely separated due to inaccurate detection of the horizontal line in the lower right corner. In the second row, the text lines in the background mislead the model's accuracy in segmenting horizontal lines.

E. Ablation studies

To validate the efficacy of our proposed *D2Dewarp*, we conduct ablation experiments. Firstly, we verify the impact of HV Fusion Module on the corrective effect. As shown in Tables V, overall, the HV Fusion Module has a positive effect on the final dewarping results, especially in improving document readability (ED and CER). The LD and AD indicators have slight fluctuations, indicating that the HV Fusion Module focuses more on document readability, and more effective fusion modules still need to be studied in the future. In addition, we further experimentally demonstrated the impact of either horizontal or vertical line features on the rectification results as shown in Table VI. In this ablation experiment, whether H-Line or V-Line is used, the same number of self-attention layers is retained to ensure fair comparison. The



Fig. 9. Qualitative visualization comparison between several methods on DocReal [28] benchmark.

result shows that the distorted image can be rectified even if one of the line is used, but the complementary features and constraints between the two lines can enhance the perception of deformation characteristics.

To investigate the impact of varying *text coverage ratio* on image rectification quality, text density was calculated using PaddleOCR on the ground truth images of the DocUNet benchmark (130 images) - as opposed to distorted images - to maximize text detection accuracy. The text coverage ratio was computed as the total area of detected text boxes relative to the entire image area. Images were sorted in ascending order by text coverage and divided into three intervals (from 0.9% to 65%): Low ($\leq 20\%$), Middle (20%-40%), and High ($\geq 40\%$) text density, as detailed in Table VII. Overall, high text density significantly impacts MS-SSIM, LD, and AD metrics. As text content increases, both MS-SSIM and AD exhibit performance degradation. We attribute this to their computational principles: in high-text-density regions, the discontinuous pixel distribution in text lines (compared to figure-heavy images) increases sensitivity to pixel mis-

TABLE V

ABLATION STUDY OF HV FUSION MODULE ON DocUNet [17], DIR300 [24] AND DocReal [28] BENCHMARKS. HV-FM IS HV FUSION MODULE. “✓” INDICATES THAT THE FEATURE FUSION MODULE OF HORIZONTAL OR VERTICAL LINES IS USED. “✗” IS THE OPPOSITE.

Benchmark	HV-FM	MS-SSIM↑	LD↓/AD↓	ED↓	CER↓
DocUNet [17]	✗ ✓	0.50 0.50	7.55/0.343 7.71/0.349	401.08 351.08	0.1439 0.1338
DIR300 [24]	✗ ✓	0.64 0.65	5.56/0.193 5.73/0.186	509.82 466.94	0.1682 0.1676
DocReal [28]	✗ ✓	0.56 0.58	9.18/0.252 8.69/0.227	199.72 191.25	0.2665 0.2588

TABLE VI

ABLATION STUDIES OF HORIZONTAL OR VERTICAL LINE (H-LINE, V-LINE) PREDICTED OR NOT ON DocREAL BENCHMARK [28].

H-Line	V-Line	MS-SSIM↑	LD↓/AD↓	ED↓	CER↓
✓	✗	0.58	9.01/0.253	197.98	0.267
✗	✓	0.57	9.00/0.243	201.12	0.265
✓	✓	0.58	8.69/0.227	191.25	0.259

alignment. Conversely, LD demonstrates opposite behavior, its performance notably improves with higher text density. This stems from text content’s inherent local characteristics, where abundant local features enhance LD’s feature matching capability.

Limitations. Our method still has some limitations. As mentioned above, distorted images in real scenes are subject to interference from text backgrounds, irregular charts without clear boundaries, which prevent our method may not effectively enhance performance. For this problem, correction performance could potentially be further enhanced by leveraging existing methods to integrate global information such as foreground features or UV maps.

V. CONCLUSION

We release the *DocDewarpHV* dataset, a warped document training set with more fine-grained annotations in both horizontal and vertical directions. We propose *D2Dewarp*, a novel approach for document image rectification that perception horizontal and vertical line features. Our method can automatically learn distortion trends across different lines end-to-end and achieve information complementarity. The lines Fusion Module (HV Fusion Module) is introduced to enhance the interaction between features from various lines, improving geometric representation learning of document deformation. Comprehensive quantitative evaluation and ablation experiments conducted on the three benchmarks demonstrate the effectiveness of our model. By considering both horizontal and vertical line, our proposed method explores the intrinsic relationships between different direction features, thereby improving the flatness and readability of warped document images. The results indicate that HV Fusion Module enhances document image dewarping performance with efficiency, achieving state-of-the-art results.

TABLE VII

IMPACT OF TEXT COVERAGE RATIO ON MS-SSIM, LD, AND AD METRICS OVER THE DocUNet [17] BENCHMARK.

Text Coverage Ratio (TCR)	MS-SSIM↑	LD↓	AD↓
$TCR \leq 20\%$	0.55	10.57	0.305
$20\% < TCR \leq 40\%$	0.48	5.97	0.375
$TCR > 40\%$	0.43	5.02	0.418

REFERENCES

- [1] M. Li, B. Fu, Z. Zhang, and Y. Qiao, “Character-aware sampling and rectification for scene text recognition,” *IEEE Transactions on Multimedia*, vol. 25, pp. 649–661, 2023.
- [2] D. Peng, L. Jin, W. Ma, C. Xie, H. Zhang, S. Zhu, and J. Li, “Recognition of handwritten chinese text by segmentation: A segment-annotation-free approach,” *IEEE Transactions on Multimedia*, vol. 25, pp. 2368–2381, 2022.
- [3] C. Yang, M. Chen, Y. Yuan, and Q. Wang, “Reinforcement shrink-mask for text detection,” *IEEE Transactions on Multimedia*, vol. 25, pp. 6458–6470, 2023.
- [4] J.-N. Li, X.-Q. Liu, X. Luo, and X.-S. Xu, “Volter: Visual collaboration and dual-stream fusion for scene text recognition,” *IEEE Transactions on Multimedia*, vol. 26, pp. 6437–6448, 2024.
- [5] X.-Q. Liu, P. Zhang, X. Luo, Z. H. Huang, and X.-S. Xu, “Textadapter: Self-supervised domain adaptation for cross-domain text recognition,” *IEEE Transactions on Multimedia*, vol. 26, pp. 9854–9865, 2024.
- [6] M. Cao and Y. Zou, “All you need is a second look: Towards tighter arbitrary shape text detection,” in *ICASSP 2020 - 2020 IEEE International Conference on Acoustics, Speech and Signal Processing (ICASSP)*, 2020, pp. 2228–2232.
- [7] P. Cheng, Y. Zhao, and W. Wang, “Detect arbitrary-shaped text via adaptive thresholding and localization quality estimation,” *IEEE Transactions on Circuits and Systems for Video Technology*, vol. 33, no. 12, pp. 7480–7490, 2023.
- [8] Z. Wang, H. Xie, Y. Wang, J. Xu, B. Zhang, and Y. Zhang, “Symmetrical linguistic feature distillation with clip for scene text recognition,” *Proceedings of the 31st ACM International Conference on Multimedia*, 2023.
- [9] J. Xu, A. Lin, J. Li, and G. Lu, “Text position-aware pixel aggregation network with adaptive gaussian threshold: Detecting text in the wild,” *IEEE Transactions on Circuits and Systems for Video Technology*, vol. 34, pp. 286–298, 2024.
- [10] H. Wei, C. Liu, J. Chen, J. Wang, L. Kong, Y. Xu, Z. Ge, L. Zhao, J. Sun, Y. Peng, C. Han, and X. Zhang, “General ocr theory: Towards ocr-2.0 via a unified end-to-end model,” *ArXiv*, vol. abs/2409.01704, 2024.
- [11] H. Fang, W. Zhang, Z. Ma, H. Zhou, S. Sun, H. Cui, and N. Yu, “A camera shooting resilient watermarking scheme for underpainting documents,” *IEEE Transactions on Circuits and Systems for Video Technology*, vol. 30, pp. 4075–4089, 2020.
- [12] Z. Jin, H. Wu, C. Yang, F. Zhou, J. Qin, L. Xiao, and X.-C. Yin, “Ruart: A novel text-centered solution for text-based visual question answering,” *IEEE Transactions on Multimedia*, vol. 25, pp. 1–12, 2020.
- [13] H. Bi, C. Xu, C. Shi, G. Liu, Y. Li, H. Zhang, and J. Qu, “Srrv: A novel document object detector based on spatial-related relation and vision,” *IEEE Transactions on Multimedia*, vol. 25, pp. 3788–3798, 2023.
- [14] H. Feng, Q. Liu, H. Liu, W. gang Zhou, H. Li, and C. Huang, “Docpedia: Unleashing the power of large multimodal model in the frequency domain for versatile document understanding,” *ArXiv*, vol. abs/2311.11810, 2023.
- [15] W. Liao, J. Wang, H. Li, C. Wang, J. Huang, and L. Jin, “Doclaylm: An efficient and effective multi-modal extension of large language models for text-rich document understanding,” *ArXiv*, vol. abs/2408.15045, 2024.
- [16] J. Zhang, W. Yang, S. Lai, Z. Xie, and L. Jin, “Docklylin: A large multimodal model for visual document understanding with efficient visual slimming,” *ArXiv*, vol. abs/2406.19101, 2024.
- [17] K. Ma, Z. Shu, X. Bai, J. Wang, and D. Samaras, “Docunet: Document image unwarping via a stacked u-net,” *2018 IEEE/CVF Conference on Computer Vision and Pattern Recognition*, pp. 4700–4709, 2018.
- [18] S. Das, K. Ma, Z. Shu, D. Samaras, and R. Shilkrot, “Dewarpnet: Single-image document unwarping with stacked 3d and 2d regression networks,” *2019 IEEE/CVF International Conference on Computer Vision (ICCV)*, pp. 131–140, 2019.

- [19] X. Liu, G. Meng, B. Fan, S. Xiang, and C. Pan, "Geometric rectification of document images using adversarial gated unwarping network," *Pattern Recognit.*, vol. 108, p. 107576, 2020.
- [20] G.-W. Xie, F. Yin, X.-Y. Zhang, and C.-L. Liu, "Dewarping document image by displacement flow estimation with fully convolutional network," *ArXiv*, vol. abs/2104.06815, 2020.
- [21] H. Feng, Y. Wang, W. gang Zhou, J. Deng, and H. Li, "Doctr: Document image transformer for geometric unwarping and illumination correction," *Proceedings of the 29th ACM International Conference on Multimedia*, 2021.
- [22] G.-W. Xie, F. Yin, X.-Y. Zhang, and C.-L. Liu, "Document dewarping with control points," in *IEEE International Conference on Document Analysis and Recognition*, 2022.
- [23] X. Jiang, R. Long, N. Xue, Z. Yang, C. Yao, and G. Xia, "Revisiting document image dewarping by grid regularization," *2022 IEEE/CVF Conference on Computer Vision and Pattern Recognition (CVPR)*, pp. 4533–4542, 2022.
- [24] H. Feng, W. gang Zhou, J. Deng, Y. Wang, and H. Li, "Geometric representation learning for document image rectification," *ArXiv*, vol. abs/2210.08161, 2022.
- [25] B. Dai, X. Li, Q. Xie, Y. Li, X. Qin, C. Zhang, K. Yao, and J. Han, "Matadoc: Margin and text aware document dewarping for arbitrary boundary," *ArXiv*, vol. abs/2307.12571, 2023.
- [26] P. Li, W. Quan, J. Guo, and D. Yan, "Layout-aware single-image document flattening," *ACM Transactions on Graphics*, vol. 43, pp. 1 – 17, 2023.
- [27] H. Li, X. Wu, Q. Chen, and Q. Xiang, "Foreground and text-lines aware document image rectification," *2023 IEEE/CVF International Conference on Computer Vision (ICCV)*, pp. 19 517–19 526, 2023.
- [28] F. Yu, Y. Xie, L. Wu, Y. Wen, G. Wang, S. Ren, X. Chen, J. Mao, and W. Li, "Docreal: Robust document dewarping of real-life images via attention-enhanced control point prediction," in *Proceedings of the IEEE/CVF Winter Conference on Applications of Computer Vision (WACV)*, January 2024, pp. 665–674.
- [29] S. Liu, H. Feng, and W. Zhou, "Rethinking supervision in document unwarping: A self-consistent flow-free approach," *IEEE Transactions on Circuits and Systems for Video Technology*, vol. 34, no. 6, pp. 4817–4828, 2024.
- [30] F. Hertlein, A. Naumann, and Y. Sure-Vetter, "Docmatcher: Document image dewarping via structural and textual line matching," in *2025 IEEE/CVF Winter Conference on Applications of Computer Vision (WACV)*. IEEE, 2025, pp. 5771–5780.
- [31] J. Zhang, P. Zhang, D. Peng, H. Xu, and L. Jin, "Enhancing document dewarping evaluation: A new metric with improved accuracy and efficiency," *Pattern Recognition Letters*, 2025.
- [32] M. Han and H. Li, "Docmamba: Robust document image dewarping via selective state space sequence modeling," in *International Conference on Multimedia Modeling*. Springer, 2025, pp. 304–318.
- [33] Z. Huang, J. Gu, G. Meng, and C. Pan, "Text line extraction of curved document images using hybrid metric," *2015 3rd IAPR Asian Conference on Pattern Recognition (ACPR)*, pp. 251–255, 2015.
- [34] T. Wada, H. Ukida, and T. Matsuyama, "Shape from shading with interreflections under a proximal light source: Distortion-free copying of an unfolded book," *International Journal of Computer Vision*, vol. 24, pp. 125–135, 1997.
- [35] F. Courteille, A. Crouzil, J.-D. Durou, and P. Gurdjos, "Shape from shading for the digitization of curved documents," *Machine Vision and Applications*, vol. 18, pp. 301–316, 2007.
- [36] J. Liang, D. DeMenthon, and D. S. Doermann, "Geometric rectification of camera-captured document images," *IEEE Transactions on Pattern Analysis and Machine Intelligence*, vol. 30, pp. 591–605, 2008.
- [37] G. Meng, Y. Su, Y. Wu, S. Xiang, and C. Pan, "Exploiting vector fields for geometric rectification of distorted document images," in *European Conference on Computer Vision*, 2018.
- [38] Y.-C. Tsoi and M. S. Brown, "Multi-view document rectification using boundary," *2007 IEEE Conference on Computer Vision and Pattern Recognition*, pp. 1–8, 2007.
- [39] M. S. Brown and Y.-C. Tsoi, "Geometric and shading correction for images of printed materials using boundary," *IEEE Transactions on Image Processing*, vol. 15, pp. 1544–1554, 2006.
- [40] H. Feng, W. Zhou, J. Deng, Q. Tian, and H. Li, "Docscanner: Robust document image rectification with progressive learning," *International Journal of Computer Vision*, pp. 1–20, 2025.
- [41] H. Feng, S. Liu, J. Deng, W. Zhou, and H. Li, "Deep unrestricted document image rectification," *IEEE Transactions on Multimedia*, 2023.
- [42] X. Li, B. Zhang, J. Liao, and P. V. Sander, "Document rectification and illumination correction using a patch-based cnn," *ACM Transactions on Graphics (TOG)*, vol. 38, pp. 1 – 11, 2019.
- [43] S. Das, K. Y. Singh, J. Wu, E. Bas, V. Mahadevan, R. Bhotika, and D. Samaras, "End-to-end piece-wise unwarping of document images," *2021 IEEE/CVF International Conference on Computer Vision (ICCV)*, pp. 4248–4257, 2021.
- [44] O. Ronneberger, P. Fischer, and T. Brox, "U-net: Convolutional networks for biomedical image segmentation," in *Medical image computing and computer-assisted intervention—MICCAI 2015: 18th international conference, Munich, Germany, October 5–9, 2015, proceedings, part III 18*. Springer, 2015, pp. 234–241.
- [45] S. Ioffe and C. Szegedy, "Batch normalization: Accelerating deep network training by reducing internal covariate shift," *ArXiv*, vol. abs/1502.03167, 2015.
- [46] V. Nair and G. E. Hinton, "Rectified linear units improve restricted boltzmann machines," in *International Conference on Machine Learning*, 2010.
- [47] Q. Hou, D. Zhou, and J. Feng, "Coordinate attention for efficient mobile network design," in *Proceedings of the IEEE/CVF Conference on Computer Vision and Pattern Recognition (CVPR)*, June 2021, pp. 13 713–13 722.
- [48] P. T. de Boer, D. P. Kroese, S. Mannor, and R. Y. Rubinstein, "A tutorial on the cross-entropy method," *Annals of Operations Research*, vol. 134, pp. 19–67, 2005.
- [49] S. Liu, H. Feng, W. gang Zhou, H. Li, C. Liu, and F. Wu, "Docmae: Document image rectification via self-supervised representation learning," *2023 IEEE International Conference on Multimedia and Expo (ICME)*, pp. 1613–1618, 2023.
- [50] X. Zhong, J. Tang, and A. Jimeno-Yepes, "Publaynet: Largest dataset ever for document layout analysis," *2019 International Conference on Document Analysis and Recognition (ICDAR)*, pp. 1015–1022, 2019.
- [51] H. Li, "CdlA: A chinese document layout analysis (cdla) dataset," 2021.
- [52] K. Li, C. Wigington, C. Tensmeyer, H. Zhao, N. Barmpalios, V. I. Morariu, V. Manjunatha, T. Sun, and Y. Fu, "Cross-domain document object detection: Benchmark suite and method," in *Proceedings of the IEEE/CVF Conference on Computer Vision and Pattern Recognition*, 2020, pp. 12 915–12 924.
- [53] H. Cheng, P. Zhang, S. Wu, J. Zhang, Q. Zhu, Z. Xie, J. Li, K. Ding, and L. Jin, "M6doc: A large-scale multi-format, multi-type, multi-layout, multi-language, multi-annotation category dataset for modern document layout analysis," in *Proceedings of the IEEE/CVF Conference on Computer Vision and Pattern Recognition (CVPR)*, June 2023, pp. 15 138–15 147.
- [54] C. Xue, Z. Tian, F. Zhan, S. Lu, and S. Bai, "Fourier document restoration for robust document dewarping and recognition," *2022 IEEE/CVF Conference on Computer Vision and Pattern Recognition (CVPR)*, pp. 4563–4572, 2022.
- [55] K. Ma, S. Das, Z. Shu, and D. Samaras, "Learning from documents in the wild to improve document unwarping," *ACM SIGGRAPH 2022 Conference Proceedings*, 2022.
- [56] F. Verhoeven, T. Magne, and O. Sorkine-Hornung, "UVDoc: Neural grid-based document unwarping," in *SIGGRAPH ASIA, Technical Papers*, 2023.
- [57] J. Zhang, D. Peng, C. Liu, P. Zhang, and L. Jin, "Docres: A generalist model toward unifying document image restoration tasks," *2024 IEEE/CVF Conference on Computer Vision and Pattern Recognition (CVPR)*, pp. 15 654–15 664, 2024.
- [58] P. Kumari and S. Das, "Am i readable? transfer learning based document image rectification," *Int. J. Document Anal. Recognit.*, vol. 27, pp. 433–446, 2024.
- [59] J. Zhang, C. Luo, L. Jin, F. Guo, and K. Ding, "Marior: Margin removal and iterative content rectification for document dewarping in the wild," *Proceedings of the 30th ACM International Conference on Multimedia*, 2022.
- [60] Z. Wang, A. C. Bovik, H. R. Sheikh, and E. P. Simoncelli, "Image quality assessment: from error visibility to structural similarity," *IEEE Transactions on Image Processing*, vol. 13, pp. 600–612, 2004.
- [61] S. You, Y. Matsushita, S. Sinha, Y.-K. Bou, and K. Ikeuchi, "Multi-view rectification of folded documents," *IEEE Transactions on Pattern Analysis and Machine Intelligence*, vol. 40, pp. 505–511, 2016.
- [62] C. Liu, J. Yuen, and A. Torralba, "Sift flow: Dense correspondence across scenes and its applications," *IEEE Transactions on Pattern Analysis and Machine Intelligence*, vol. 33, pp. 978–994, 2011.
- [63] I. Loshchilov and F. Hutter, "Decoupled weight decay regularization," in *International Conference on Learning Representations*, 2017.

- [64] R. W. Smith, “An overview of the tesseract ocr engine,” *Ninth International Conference on Document Analysis and Recognition (ICDAR 2007)*, vol. 2, pp. 629–633, 2007.